RESEARCH PAPER

Wear Properties of Al/MoS_2 Nanocomposite Coatings Generated by Electro-Spark Deposition on the Surface of Ti-6Al-4V Alloy

Mohammad Roostaei[1], Hossein Aghajani[2,]*, Majid Abbasi[3], Behzad Abasht[4]

** haghajani@iust.ac.ir*

[1] Department of Materials Engineering, University of Tabriz, Tabriz, Iran
[2] School of Metallurgy and Materials Engineering, Iran University of Science and Technology, Tehran, Iran
[3] Department of Materials Engineering, Babol Noshirvani University of Technology, Babol, Iran
[4] Space Thrusters Institute, Tabriz, Iran

Received: January 2022 **Revised: February 2022** **Accepted: March 2022**

DOI: 10.22068/ijmse.2639

Abstract: *This study investigates the effect of Al/MoS_2 nanocomposite coating by the electro spark deposition (ESD) method on the surface properties of the substrate. Ti-6Al-4V alloy sheet containing 6.12% Al, 4.06% V, 0.19% Fe, and 0.05% Ni was used as substrate in this study. For coating, an aluminum-molybdenum disulfide composite electrode in the form of a cylindrical rod was employed. Three frequencies of 5, 8, and 11 kHz, three current limits of 15, 25, and 35 amps, and three duty cycles of 50, 60, and 70% were used in the coating operation. AFM analysis was used to study the topography, morphology, and to calculate roughness. The samples were then subjected to hardness tests. To determine the wear resistance of the samples, pin on disk tests were performed. XRD analysis was performed to identify the phases on the surface of the coated samples. SEM was used to examine the microstructure of the coating before and after wear testing, in order to determine the wear mechanism. The results indicated that the Al/MoS_2 nanocomposite coating was formed on the substrate surface. The hardness of the reference sample was 353 Vickers, and that of the coated sample was about 200 Vickers. For the reference sample, the roughness was measured at 15.7 nm, and for the coated sample at 268.1 nm. As spark energy increased, the coefficient of friction increased by approximately 0.09. As spark energy increased, the wear rate increased by 27%. A significant increase in the Lancaster coefficient occurred around 5 joules of energy. According to the wear rate results, the sample with the lowest thickness wears 4% less than the sample with the highest thickness. The wear rate of sample 351170 is 78% lower than that of sample 150550.*

Keywords: *Al/MoS_2 nanocomposite coating, electro spark deposition, wear properties, Synthesis.*

1. INTRODUCTION

The most widely used titanium alloy is grade 5 titanium, also known as Ti-6Al-4V (Ti 6-4). Titanium has a low density and high strength, but its wear resistance is weak. The coating is one of the ways to improve the physical and mechanical properties of various metal parts. Various coatings are created with different thicknesses and conditions depending on the application. In the coating process, abrasion is one of the most important properties to be considered [1–5]. Due to the low wear resistance of parts in various conditions, these parts perform improperly, resulting in additional damage and costs.

Therefore, various coatings have been proposed to improve the abrasion properties of metals and alloys. Different methods have also been studied for applying these coatings. To obtain abrasion-resistant coatings on titanium substrates and their alloys, various methods have been employed, including magnetic sputtering, laser deposition, physical vapor deposition, mechanical alloying, anodizing, powder metallurgy, electrical spark deposition, etc [6–10]. In a study, Tijo et al investigated a TiC/TiB_2 composite coating on a Ti-6Al-4V substrate. Based on the results of the sliding wear test, the coatings have more wear resistance than the sample without coating. In particular, this is due to the properties of composite coatings in which TiC and TiB ceramic compounds are evenly distributed and thus their hardness is significantly increased. Consequently, composite coatings have excellent abrasion properties due to their excellent resistance to micro-shear and abrasion during the dry sliding wear process [11].

Some places cannot be lubricated with ordinary lubricants, such as space. In space, due to the lack of gravity and the existence of a vacuum, it is not possible to use liquid lubricants, etc. Thus, one of the greatest challenges in the design of parts used in space that require lubrication is selecting the right material to replace conventional lubricants

[DOI: 10.22068/ijmse.2639]

with self-lubricating properties. Molybdenum disulfide is one of these materials that has self-lubricating properties. It consists of layers of Mo-S-Mo, which are very weak van der Waals bonds. This bond provides graphite with its lubricating properties. The finer the lubricant particles and the more uniform their distribution, the easier they will penetrate the wear surface and reduce the coefficient of friction further [12–18]. Kanthavel et al. [19] synthesized aluminum/ alumina/ molybdenum disulfide composites by powder metallurgy. Creating a coating improved the wear properties of the substrate. Yunfeng et al. [20] have developed an in situ synthesized self-lubricating composite of Al_2O_3/ MoS_2 with molybdenum disulfide nanoparticles. The results indicate that the coefficient of friction decreased. Molybdenum disulfide is known for its automotive properties, which reduce friction coefficients and enhance wear resistance. An investigation by Li et al. [21] explored the lubrication characteristics of a composite coating of C-Ti/ MoS_2 created by magnetron sputtering on stainless steel 304 substrates. According to the results, the formation of this coating increased the hardness of the substrate, which resulted from the increased modulus of elasticity. The presence of MoS_2 in the coating creates self-lubricating properties, resulting in reduced coefficients of friction and improved abrasion properties. Another study investigated the tribological properties of MoS_2/Zr composite coatings by Li et al. [22] The coating was created on a 304 stainless steel substrate by magnetron sputtering. Due to the multilayer structure of the coating, the coefficient of friction decreased and the abrasion resistance increased. Additionally, Zhi Jing Peng et al. [23, 24] investigated the formation of a MoS_2/Al_2O_3 composite coating on the A356 alloy to reduce friction. Due to the presence of molybdenum disulfide as a solid lubricant, coated samples showed lower coefficients of friction.

Electro spark deposition (ESD) is a pulsed coating method that is used for small-scale and precision repair of special components. ESD is also known as spark hardening, electro spark toughening, electro spark alloying, pulsed fusion surfacing, and pulsed electrode surfacing. Electro spark deposition systems contain a direct current power supply that produces pulses through a rotating electrode. The consumable electrode material is deposited onto the work piece by means of sparks. In the electro spark deposition process, the electrode is the anode and the work piece is the cathode. When the spark energy is released, the direct current generates a plasma arc at a high temperature (8000 to 25,000°C) between the tip of the electrode and the work piece. The plasma arc ionizes the electrode material and a small quantity of molten electrode material is transferred onto the work piece. The transfer of material is rapid and the self-quenching is extremely fast. Based on short duration, high current pulses, the process imparts a low heat input to the substrate material, resulting in little or no modification of the substrate microstructure. Therefore, the process offers an advantage over fusion welding processes (including arc, laser and resistance welding) when repairing materials that are difficult to weld because of very small heat affected zone faults (e.g. liquation cracking, high hardness, low toughness). Components can be restored to their original dimensions, because with such low heat input the bulk substrate material remains near to ambient temperature with thermal distortion, shrinkage, and high residual stresses avoided. Moreover, the process generates a good metallurgical bond between the coating and the substrate. Electro spark deposition is particularly suitable for the repair of small and shallow defects, but it is not appropriate for large defects, since the process is slow and the maximum thickness of the coating is about 2 mm. Electro spark deposition can also be considered as a process to increase the wear and the erosion resistance of small surface areas. During this process, due to the high melting and freezing speeds, the substrate structure is not damaged, but its surface properties are improved [25, 26]. One of the main uses of the electro spark deposition method is to increase wear resistance, a subject that has been examined in numerous studies. It is also possible to improve and increase the surface hardness with this method [27]. Hong et al.[28] Applied TiN coatings to titanium alloy substrates using electro-spark deposition in order to enhance the tribological properties of titanium alloys. Microhardness tests indicated an increase in surface hardness. Also, the results of friction and wear of TiN coatings showed that the amount of weight loss, as well as friction coefficients for samples with coating, is less than TC11 substrate. Micro-wear is primarily caused by cutting and plastic deformation[28]. In a study on a titanium

[DOI: 10.22068/ijmse.2639]

substrate, Tang et al. [29] applied a wear-resistant graphite coating by electro-spark deposition. In this study, the coating of Al/MoS_2 nanocomposite on a Ti-6AL-4V substrate was synthesized by the electro-spark deposition method. As a result of its self-lubricating properties, molybdenum disulfide was selected to improve tribological properties. The lubricating properties of Al/MoS_2 nanocomposite coatings, including their hardness and wear properties, are examined.

2. EXPERIMENTAL PROCEDURES

2.1. Workpiece and electrode

Samples were cut into 30 by 30 mm^2 using a wire cut to perform the coating process. The samples were sanded up to 1500 mesh and polished. The electrode used in the ESD method is cylindrical. An electrode was prepared using 95% weight of aluminum powder (Sigma-Aldrich, Germany) with a purity of 99.9% and a size of 30 micrometers and 5% by weight of molybdenum disulfide powder (Sigma-Aldrich, Germany) with a purity of 99.9 and less. They were milled and mixed at 500 nm for 8 hours with a ball to powder ratio of 1:20 in the presence of ethanol. The powder was placed in a cylindrical mold with a diameter of 4 mm and a height of 40 mm and pressed under a pressure of 10 KN. The crude electrodes were placed under an argon atmosphere at 500° C for 8 hours for sintering in a tube furnace.

2.2. ESD process

The used conditions are mentioned in sample coding. Sample codes consist of a 6-digit number, which the first two digits are related to the current limit (15, 25, or 35 A), the second two digits are related to Frequency (5, 8, or 11 kHz), and the last two digits determine the duty cycle (50, 60, or 70%). For example, 150550 sample is coated at the current limit of 15 A, frequency of 5 kHz, and duty cycle of 50%.
Table (1) shows the samples' codes and their coating conditions.

Table 1. shows the samples' codes and their coating conditions

Sample code	Current limit (A)	Frequency (kHz)	Duty cycle (%)
150550	15	5	50
250550	25		
250550	35		
150850	15	8	
250850	25		
350850	35		
151150	15	11	
251150	25		
351150	35		
150560	15	5	60
250560	25		
350560	35		
150860	15	8	
250860	25		
350860	35		
151160	15	11	
251160	25		
351160	35		
150570	15	5	70
250570	25		
350570	35		
150870	15	8	
250870	25		
350870	35		
151170	15	11	
251170	25		
351170	35		

[DOI: 10.22068/ijmse.2639]

2.3. Characterization

Atomic force microscope (AFM) with a tip made of Si_3N_4 was used to study the topography, morphology, and calculation of roughness and other dimensional parameters of surface particles. To determine the wear resistance of the samples, the wear test was performed by a pin on disk method. As a result of the testing, friction coefficient diagrams and weight loss data were recorded.

This test was performed according to the ASTM G99 standard. These conditions were selected for the test: applied vertical force 300 g, radius of rotation 10 mm, distance traveled 100 m at 60 RPM, Ti-6Al-4V pin with flat tip diameter 3 mm, and hardness 340 Vickers. Before the test, the samples were weighed. The weight was determined using a scale that was accurate to 0.1 mg. The abrasion device transmits and records 10 data per second to the software during the test, and a friction coefficient diagram appears simultaneously.

Only the reference sample was used to determine the wear load. The reason for this was to use a load for wear tests in which the reference sample withstands relatively severe wear, but the coated specimens have less wear. For this purpose, first at a constant abrasion distance of 50 m, the abrasion load was increased from the initial amount of 100 g to determine the point of change in the abrasive mechanism. Therefore, using the weight of the abrasive material and the density of the tested material, the abrasion volume was calculated for each applied load.

The density of the reference sample (titanium alloy sample) used to calculate the wear rate was 4.43 g/cm^3. The wear rate in the reference sample increases after the load of 300 g and goes out of the initial state. It seems that the reference sample shows a change in wear behavior this time. Therefore, the selected load for other fixed load tests should be equal to or less than 300 g. According to these cases, a constant load of 300 g (approximately 3 Ns) was selected as the load for the next experiments. According to the selected load, this time the coated specimens probably have abrasive behavior and the reference specimen also has adhesive and abrasive behavior.

X-ray diffraction (XRD) was used to identify the phases on the surface of the coated samples. SEM was used to examine the microstructure of the coating both before and after the wear test and to determine the wear mechanism. Samples were then tested for hardness. As a first step, to measure the hardness of the coating, a force of 50 grams was applied for 15 seconds, and the surface hardness of the samples was reported in Vickers (HV 0.05).

3. RESULTS AND DISCUSSION

3.1. SEM and XRD examinations

Figure 1 shows the SEM images of the sample surface with the thickest coating and electrode. Molybdenum disulfide particles are dispersed in an aluminum background. As shown in the figure, the coating surface has surface cracks. There is also some porosity in the coating. The mechanism of the formation of a ceramic/ metal composite (Fig 1. B) is to achieve good contact between the Al and MoS_2 powders at the interface.

The driving force for the formation of a high-strength interface is the reduction in the free energy. In order to reduce the free energy, both surfaces have to be brought into good contact, which is usually accomplished by controlling the pressure, temperature, and atmosphere during electrode production. The application of pressure results in a displacement of impurities and adjustment of irregularities due to localized deformation.

Figure 2 shows the XRD pattern of the sample with the thickest composite coating (sample 250860) compared to the primary powders. In this figure, Al-related peaks can be seen in the presence of MoS_2 peaks.

The results confirm the formation of the Al-MoS_2 composite coating, because the peaks of both materials are present in the XRD pattern. Also, some low height peaks of aluminum oxide could be distinguished. As should be noted, the presence of weak peaks corresponding to the Al_2O_3 phase in the sample is the result of the activated pure aluminum powder, which absorbs oxygen from the atmosphere and causes partial oxidation of the powder surface. As the phases in the other samples are similar to the same sample, their X-ray diffraction patterns were not considered.

[DOI: 10.22068/ijmse.2639]

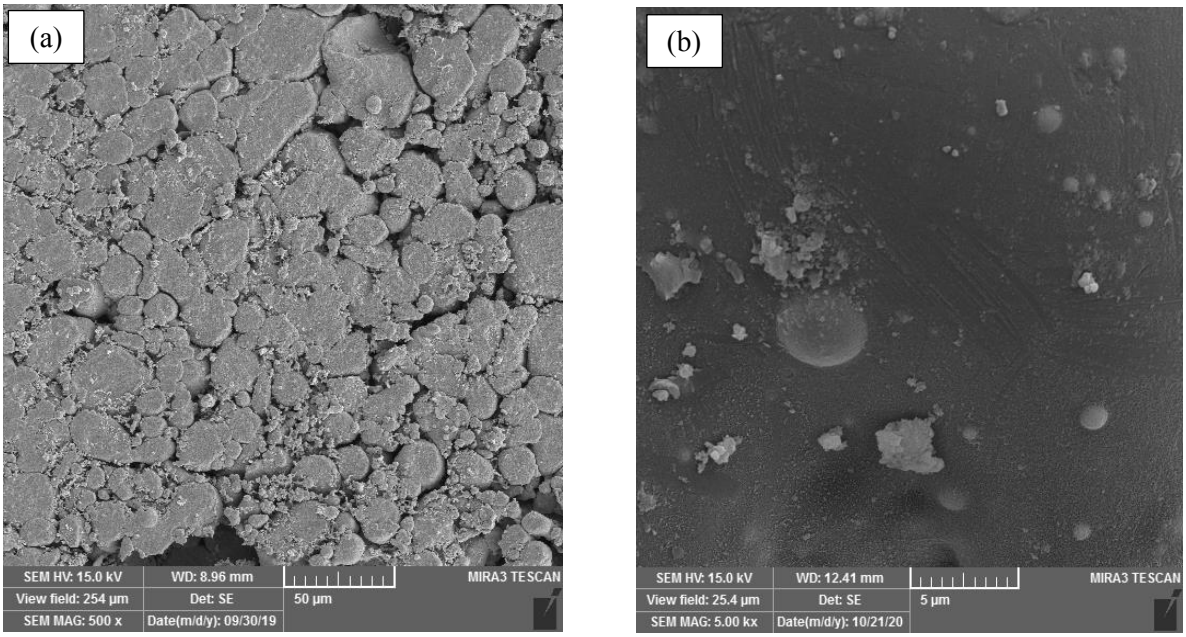

Fig. 1. SEM images of the (a) electrode microstructure and (b) the coated sample surface with the highest thickness (250860).

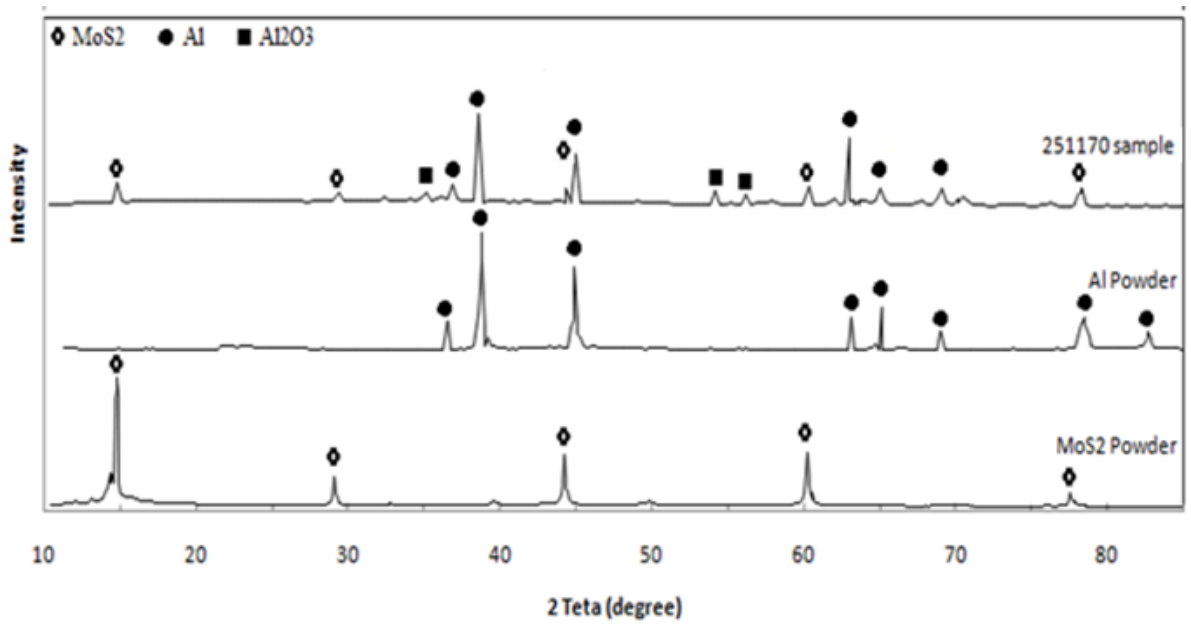

Fig. 2. XRD pattern of the sample with the highest thickness (250860) in comparison to the primary powders.

3.2. Microhardness analysis

In Figure 3, we depict the graph of hardness changes as a function of spark energy. According to the figure, the surface hardness of the samples generally decreases with the coating, compared to the reference sample. The hardness of the reference sample was approximately 353 Vickers, whereas the surface hardness of nearly all samples with coatings was approximately 200 Vickers. This was a predictable outcome. Generally, the Al-MoS_2 coating is less hard than the titanium substrate. It is apparent that regardless of the stiffness of the substrate, at first, the stiffness decreases with a uniform downward trend. In contrast, the stiffness rate decreases near the energy of 4 joules, while in the range of 4-9 joules, the stiffness remains almost constant. In order to justify this issue, two factors must be considered. First, as energy and thickness increase, the amount of soft coating deposited on

[DOI: 10.22068/ijmse.2639]

the surface increases, therefore, an increase in surface hardness can be expected. At energies higher than 4 joules, the thickness practically does not change, so the hardness remains almost constant. At energies, less than 4 joules, the coating thickness decreases, and the surface hardness increases. In thin coatings, the surface hardness is greater than the actual hardness of the coating. Additionally, as the spark energy increases, the amount of Al and MoS_2 on the surface increases.

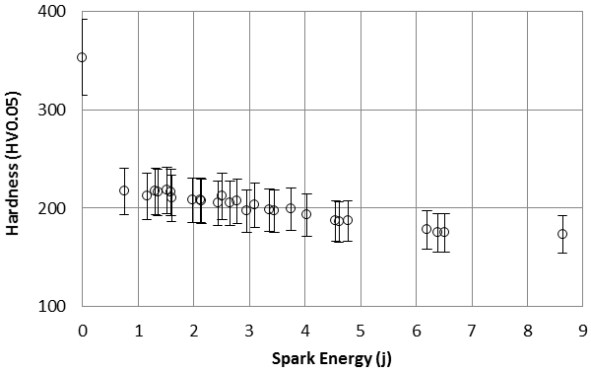

Fig. 3. Changes in surface hardness of coated samples as a function of changes in spark energy.

By increasing the amount of these two phases on the surface, it is reasonable to conclude that the surface hardness decreases. The results of the chemical composition of the surface showed that the amount of Al and Mo on the surface also increased. This factor can also contribute to a reduction in surface hardness. The presence of surface porosity is one reason why surface hardness is lower than the hardness of the substrate. The presence of porosity on the surface can make the effect of hardness appear larger, and as a result, the amount of hardness on the surface is smaller. The higher the spark energy, the greater the spray of melt on the surface, and as the spray on the surface increases, the greater the probability of surface porosity.

Surface hardness is affected by the rapid solidification of molten aluminum on the surface. During rapid freezing, the size of the surface grains becomes very small. According to the Hall-Petch relationship, this can lead to an increase in stiffness, but this increase is not very noticeable at the cross-section of the coating and near the coating-substrate interface. A good example of this can be seen in figure 4, which illustrates the hardness profile of two samples coated with the lowest spark energy (150550) and the sample coated with the highest spark energy (351170). Thus, the hardness measured in the section is initially less than the surface hardness, and increases as it moves away from the surface and closer to the joint. The increase in hardness compared with the surface hardness occurs at approximately 5 μm, which corresponds to the thickness of the sample coating. At a distance of 10-20 micrometers, a significant increase in hardness is observed and the cross-sectional hardness exceeds the surface hardness. As the hardness of these areas is lower than the stiffness of the substrate, this lower hardness may depend on the coarseness of the titanium in the heat-affected zone (HAZ) region. With annealing, the grain size increases, and the hardness decreases. With increasing depth, the stiffness approaches the stiffness values of the substrate. This indicates that depths greater than 20 μm are not affected by the coating process.

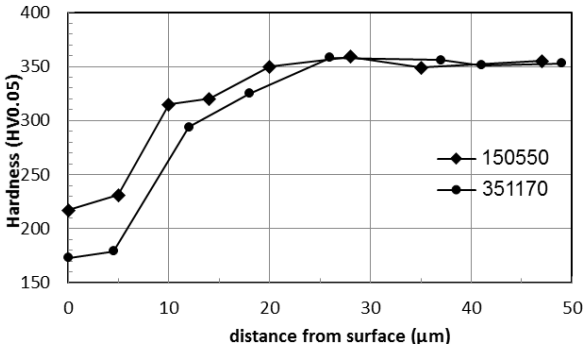

Fig. 4. Hardness changes from the surface to the depth of two coated samples with the lowest (150550) and highest (351170) spark energy.

3.3. AFM analysis

All samples were examined using an atomic force microscope (AFM). Examples of the obtained images are shown in Figure 5. The surface roughness (Sa) of the samples was determined using atomic force microscopy images. The results are shown in Figure 6. During the sparking process, materials are melted and transferred from the electrode to the surface. As a result of its adhesion to the surface, it appears necessary to study these changes. Considering that the surface roughness parameter is one of the factors associated with determining the surface texture, it can be of great assistance in solving this problem. Roughness is defined as the deviations of a true surface perpendicular to the surface from the

[DOI: 10.22068/ijmse.2639]

mean line of elevation and its elevations. In the case of large deviations, the surface is rough, and in the case of small deviations, the surface is smooth. Additionally, it should be noted that rough surfaces wear faster and have a higher coefficient of friction than smooth surfaces. Further, surface roughness is an important component in determining wear mechanisms, as this is typically the location where cracks begin. Finally, roughness can weaken the adhesion of two surfaces to each other.

Figure 6 illustrates the relationship between surface roughness and spark energy. Although the scatter in the obtained numbers is considerable, the general trend indicates that surface roughness increases with increasing spark energy. By increasing the spark energy, the splashing of molten droplets increases. So, molten droplets cannot flow on the surface and solidify rapidly. This rapid solidification makes many tops and heals on the surface and increases the roughness.

The Roughness values range from 15.7 nm for the reference sample (which has a polished surface) to 268.1 nm for the coated sample at the highest spark energy (351170). In the figure 6, the scattering roughness is much less at low spark energies (0-2 joules) and high spark energies (6-9 joules) than at medium spark energies (2-6 joules). The problem may be related to how the surface is filled. Therefore, at low energies, the surface is not completely filled, or an island morphology appears on the surface. As the spark energy increases to medium levels, the surface fills up. A layer is formed on the surface when the energy of the spray is high. The high amount of energy in the spray may cause the spark from the surface to increase, resulting in the formation of new islands. The amount of material transferred from the electrode increases as the spark energy increases. All of this material will increase the roughness of the surface with an upward trend if it is in contact with the surface.

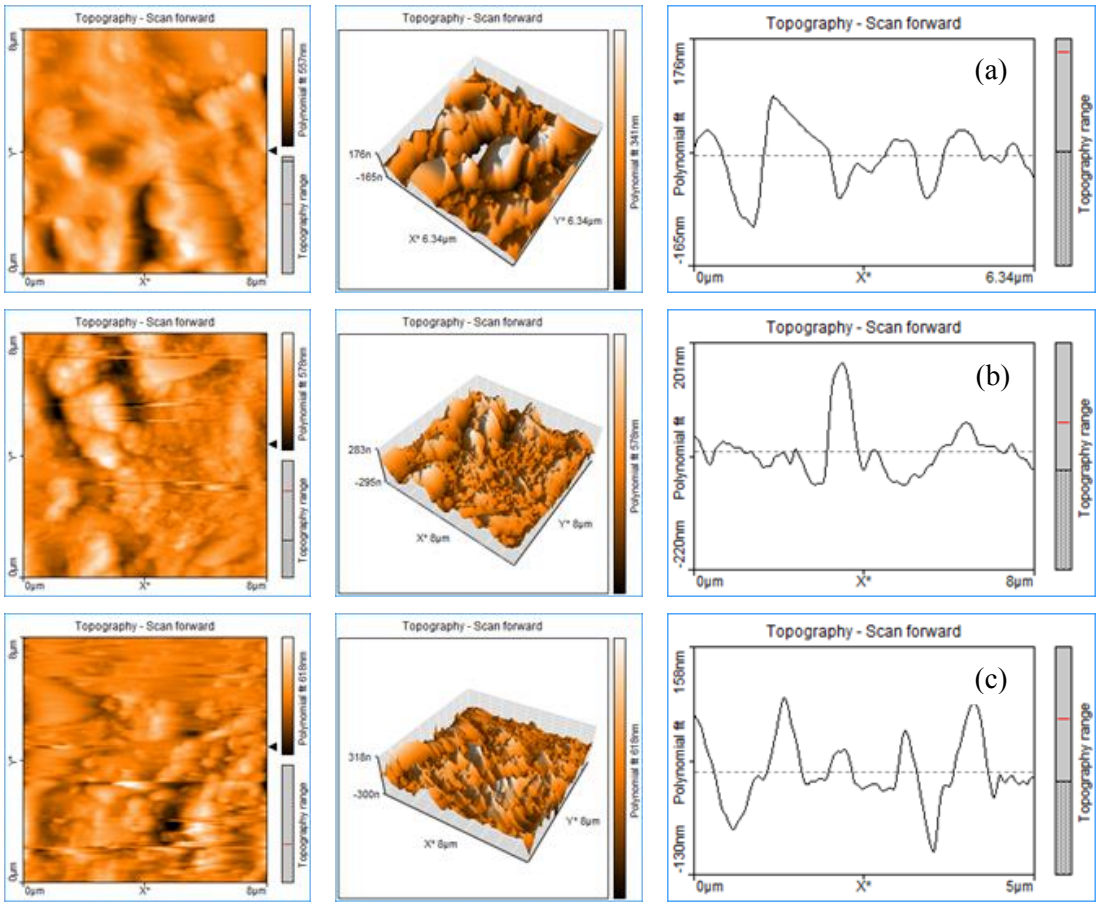

Fig. 5. Atomic force microscope results using the surface of reference specimens (a), with the highest thickness (251170) (b) and the highest spark energy (351170) (c).

[DOI: 10.22068/ijmse.2639]

Where the surface roughness has decreased locally, it is important to increase the fluidity of the melt on the surface. Spark energy increases heat transfer to the surface, and as a result, the fluidity of the melt surface also increases. The melting temperature increases melt fluidity. As the MoS_2 particles sink into the melt, the surface roughness decreases. Sparks produce a strong current of ionized and non-ionized material that hits the surface. If the surface does not have the required adhesion, the arc can result in depressions in the surface and make the surface rougher. In the absence of proper adhesion, the spray from the surface will also increase, as was mentioned earlier. However, due to the high fluctuations in roughness measured by the AFM (Figure 5), the surface of the reference specimens, the specimen with the highest thickness (251170), and the coated specimen was decided to be covered for a more detailed examination of the roughness results. Examine the maximum spark energy (351170) using scanning electron microscopy (SEM) and software. To obtain accurate information about the topographic features of the surface, images of different parts of the surface were prepared for each sample.

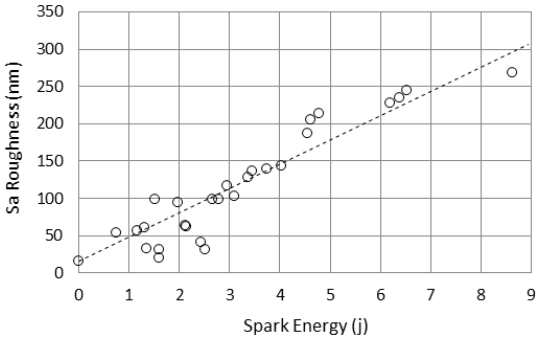

Fig. 6. Changes in surface roughness with spark energy

The measurements are made on these images, and the results are presented in Table 2. As can be seen, the roughness obtained from all samples is almost the same as the roughness obtained from an AFM microscope. Only the numbers obtained from SEM are slightly higher than those obtained from AFM. AFM determines the movement of the needle on the surface topography, and the accuracy of this determination is related to the sharpness of the needle tip. The surface topography of a surface is determined by the color distinction between raised and sunken points in the secondary electron mode (SE). Specifically, the software of this microscope measures the roughness of the image by referring to color distinction and calculates the roughness by accurate image analysis.

Table 2. Surface roughness changes obtained from AFM and SEM microscopes.

Sample	Surface roughness(S_a) (nm)	
	AFM	SEM
Sample reference	15.7±1.4	16.3±3.2
251170	228.3±3.2	229.8±5.2
351170	268.7±4.0	278.3±1.8

3.4. Wear test

3.4.1. Check the wear pin

Accordingly, the pin used was made of a substrate (Ti-6Al-4V alloy). According to the hardness test results, the pin used has a hardness of approximately 373 Vickers. Based on the fact that sample 350550 has the highest surface hardness, the pin hardness is higher than all the other samples. Figure 7 shows the pin surface image before use in the test, after 50 m of wear on the reference sample at a constant load of 300 g of force and after 50 m of wear on the reference sample at a constant load of 500 g of force.

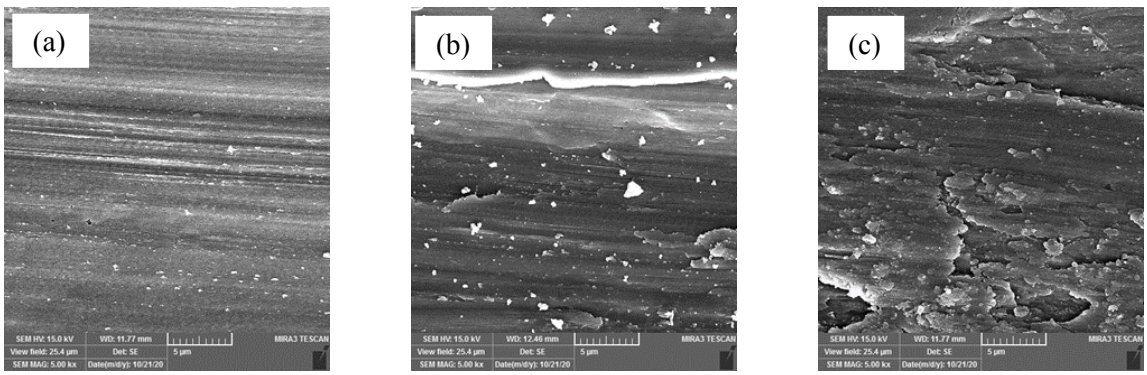

Fig. 7. The pin surface has been shown as follows: a) before the wear test, b) after 50 m wear on the reference sample at a constant load of 300 g, and c) after 50 m wear on the reference sample at a fixed load of 500 g.

[DOI: 10.22068/ijmse.2639]

It can be seen that before wear, there are only turning lines on the surface of the pin (Figure 7a). At a constant loading of 300 grams of force (Figure 7b), only a slippery effect was created on the pin surface, and abrasion did not result in severe surface deformation or peeling of large particles. Therefore, it is likely that there is no sticky abrasion but only abrasive abrasion this time. After abrasion at a load of 500 g of force, however, the pin surface (Figure 7c) suffers from abrasion and scratches, which indicates sticky abrasion between the pin and the sample. Abrasive particles on the pin's surface may also contribute to this problem.

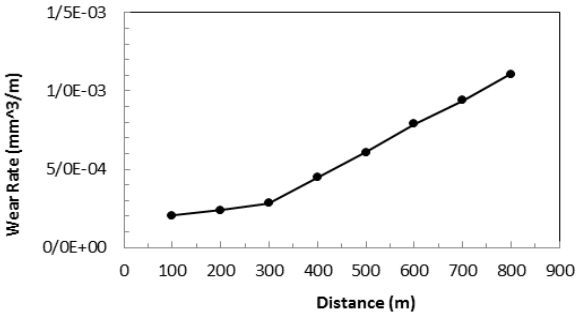

Fig. 8. Determining the point of change of abrasion mechanism from slippery abrasion to abrasive abrasion by determining the abrasion rate at different loads at a fixed slip distance of 50 m.

3.4.2. Determination of wear load

Only the reference sample was used to determine the wear load. The reason for this was to use a load for abrasion tests in which the reference sample withstands relatively severe wear, but the coated specimens have less wear. For this purpose, first, at a constant abrasion distance of 50 m, the abrasion load was increased from 100 g to determine when there is a change in the abrasion mechanism. Therefore, by measuring the weight of the abrasive material and the density of the test material, the wear volume was calculated for each applied load. The density of the reference sample (titanium alloy sample) used to calculate the wear rate was 4.43 g/cm^3. From the division of the worn volume (in mm^3) by the wear distance (in m), the wear rate (in mm^3/m) is calculated. The wear volume is obtained from the formula $V= m/\rho$ in which V is the worn volume, ρ is the density of the worn sample in terms of g/cm^3 , and m is the amount of mass reduction of the worn sample. Figure 8 illustrates the results for determining the point of change of the wear mechanism. As shown in this figure, the wear rate in the reference sample increases after a 300 g force is applied and departs from its initial pattern. It seems that the reference sample at this time shows a change in wear behavior. Therefore, the selected load for other fixed load tests should be equal to or less than 300 g of force. According to these cases, a constant load of 300 g of force (approximately 3 N) was selected as the load for the next experiments. According to the selected load, this time the coated samples probably have abrasive behavior, and the reference sample also has sticky and scratch abrasive behavior. The samples were taken out of the machine and weighed with a digital scale with an accuracy of 0.0001 g at a distance of 50 meters, and the results can be seen below.

3.4.3. Investigation of abrasion results of reference sample

Using the worn weight and the density of the reference sample (4.43 g/cm^3), the wear volume was calculated for each applied load shown in Figure 9. According to this figure and the amount of weight loss and volume reduction of the reference sample after sliding for 50 meters at 100 to 900 g of force, Lancaster wears coefficient was calculated and the results are shown in Table 3.

Table 3. Values of weight loss, volume reduction, Lancaster coefficient, and wear rate calculated for reference sample wear under different loads and a wear distance of 50 meters.

Operating load (gF)	Weight loss (mg)	Volume reduction (cm^3)	Lancaster coefficient	Abrasion rate (mm^3/m)
100	45	1.02e-02	6.51e-07	2.03e-04
200	53	1.20e-02	3.83e-07	2.39e-04
300	63	1.42e-02	3.04e-07	2.84e-04
400	99	2.23e-02	3.58e-07	4.47e-04
500	135	3.05e-02	3.91e-07	6.09e-04
600	175	3.95e-02	4.22e-07	7.90e-04
700	208	4.70e-02	4.30e-07	9.39e-04
800	245	5.53e-02	4.43e-07	1.11e-03

[DOI: 10.22068/ijmse.2639]

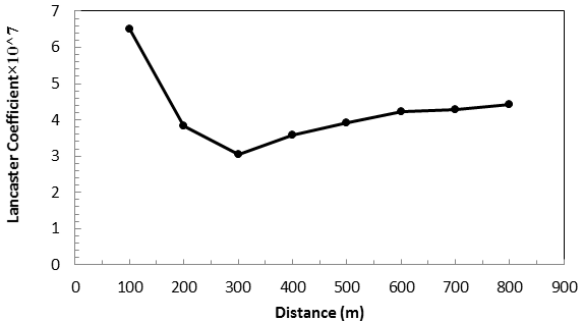

Fig. 9. Changes in Lancaster coefficient in reference sample wear under different loads and distances of 50 m.

Archard equation was used to determine the Lancaster wear coefficient [30]:

$$V = k\frac{W\,L\tan\frac{\theta}{2}}{\pi\,H} \quad (1)$$

Which:

V: Wear volume equal to m/ρ (mm^3)

k: Dimensional wear coefficient without dimension

W: Applied vertical load (N)

L: wear distance (m)

θ: pin angle with a disc (90 degrees) and

H: Disk hardness (N/mm^2)

Given o90= θ, Equation 3-1 can be rewritten as follows:

$$Q = \frac{V}{L} = \frac{k}{H} \times \frac{W}{\pi} = k' \times \frac{W}{\pi} \quad (2)$$

Where in:

Q: Abrasion rate (mm^3/m) and

k': Lancaster coefficient (equal to k/H and k is dimensionless wear coefficient, and H is the sample hardness (N/mm^2 .

The advantage of using the Lancaster wear coefficient instead of the Archard wear coefficient (dimensionless wear coefficient) is that there is no need for hardness values of the worn material anymore. Therefore, Q and k' are easily calculated at different loads (Table 4). The change curve k 'with the applied load is presented in Figure 9.

In addition to determining the abrasion load, the abrasion behavior and changes in the coefficient of friction of the reference sample are investigated. Figure 10 shows the changes in the coefficient of friction of the reference sample at a constant load of 300 g of force and a slip distance of 50 m. The scatter of the calculated values for the coefficient of friction can indicate the separation of abrasive particles from the surface and their movement in the abrasion path [31]. In other words, these fluctuations indicate the production of abrasion chips during the wear process. Based on the measurements, the friction coefficient of the reference sample is approximately 0.59. These values are in good agreement with those obtained by other researchers [32, 33].

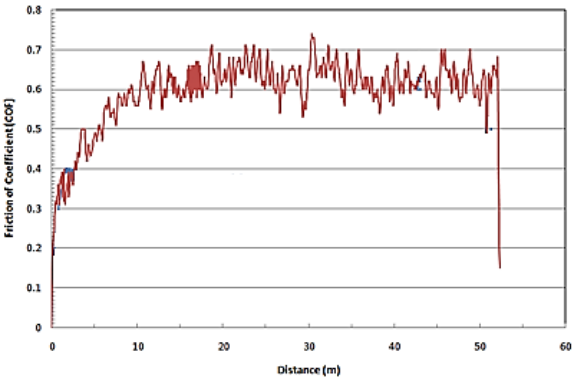

Fig. 10. Changes in the friction coefficient of the reference sample in wear under a load of 300 g force and a distance of 50 m.

As shown in Figure 11, the reference sample had a relatively uneven surface before wear. The wear surface of the reference sample is relatively smooth, and it is evident that abrasive wear is the dominant process. However, in certain places, there are bumps that are the result of the adhesive wear mechanism (Figure 11b).

3.4.4. General wear results

All coated specimens were subjected to abrasion testing. The results of these tests are presented in Table 4. According to the weight loss and density theory measurements of the coating (2.818 g/cm^3), the wear volume was calculated using the Lancaster coefficient 3 and the wear rate for each sample.Based on a brief review of the changes in various parameters, it is evident that the wear rate has increased with increasing spark energy. For a greater understanding, all the presented changes were plotted.

Figure 12 illustrates the change in friction coefficient as a function of spark energy. As can be seen in this figure, the coefficient of friction increases as spark energy increases, and the amount of increase is 0.09 and approximately 25%. It seems that with increasing spark energy and spraying of molten droplets, the possibility of MoS_2 particles separating from the surface increases.

[DOI: 10.22068/ijmse.2639]

Table 4. The values of weight loss, volume reduction, Lancaster coefficient, and wear rate calculated for the wear of different samples at a load of 300 g force and a wear distance of 50 m.

sample code	Spark energy (J)	friction coefficient	Weight loss (mg)	Volume reduction (cm^3)	Lancaster coefficient	Abrasion rate (mm^3/m)
Ref	0	0.59	63	1.42e-02	3.04e-07	2.84e-04
150550	0.75	0.36	32	1.14e-02	2.43e-07	2.27e-04
250550	1.31	0.36	33	1.17e-02	2.50e-07	2.34e-04
350550	1.52	0.33	31	1.10e-02	2.35e-07	2.20e-04
150850	1.16	0.39	35	1.24e-02	2.65e-07	2.48e-04
250850	1.97	0.41	37	1.31e-02	2.80e-07	2.63e-04
350850	2.78	0.41	37	1.31e-02	2.80e-07	2.63e-04
151150	1.60	0.42	36	1.28e-02	2.73e-07	2.56e-04
251150	2.43	0.42	37	1.31e-02	2.80e-07	2.63e-04
351150	3.75	0.42	38	1.35e-02	2.88e-07	2.70e-04
150560	1.35	0.37	33	1.17e-02	2.50e-07	2.34e-04
250560	2.12	0.42	37	1.31e-02	2.80e-07	2.63e-04
350560	3.10	0.42	38	1.35e-02	2.88e-07	2.70e-04
150860	2.14	0.41	37	1.31e-02	2.80e-07	2.63e-04
250860	3.45	0.43	40	1.42e-02	3.03e-07	2.84e-04
350860	4.77	0.44	40	1.42e-02	3.03e-07	2.84e-04
151160	2.95	0.43	40	1.42e-02	3.03e-07	2.84e-04
251160	4.61	0.44	41	1.45e-02	3.11e-07	2.91e-04
351160	6.52	0.45	41	1.45e-02	3.11e-07	2.91e-04
150570	1.59	0.37	33	1.17e-02	2.50e-07	2.34e-04
250570	2.65	0.42	38	1.35e-02	2.88e-07	2.70e-04
350570	4.03	0.43	39	1.38e-02	2.96e-07	2.77e-04
150870	2.51	0.38	34	1.21e-02	2.58e-07	2.41e-04
250870	4.55	0.44	41	1.45e-02	3.11e-07	2.91e-04
350870	6.39	0.45	42	1.49e-02	3.18e-07	2.98e-04
151170	3.36	0.43	39	1.38e-02	2.96e-07	2.77e-04
251170	6.19	0.45	40	1.42e-02	3.03e-07	2.84e-04
351170	8.63	0.45	41	1.45e-02	3.11e-07	2.91e-04

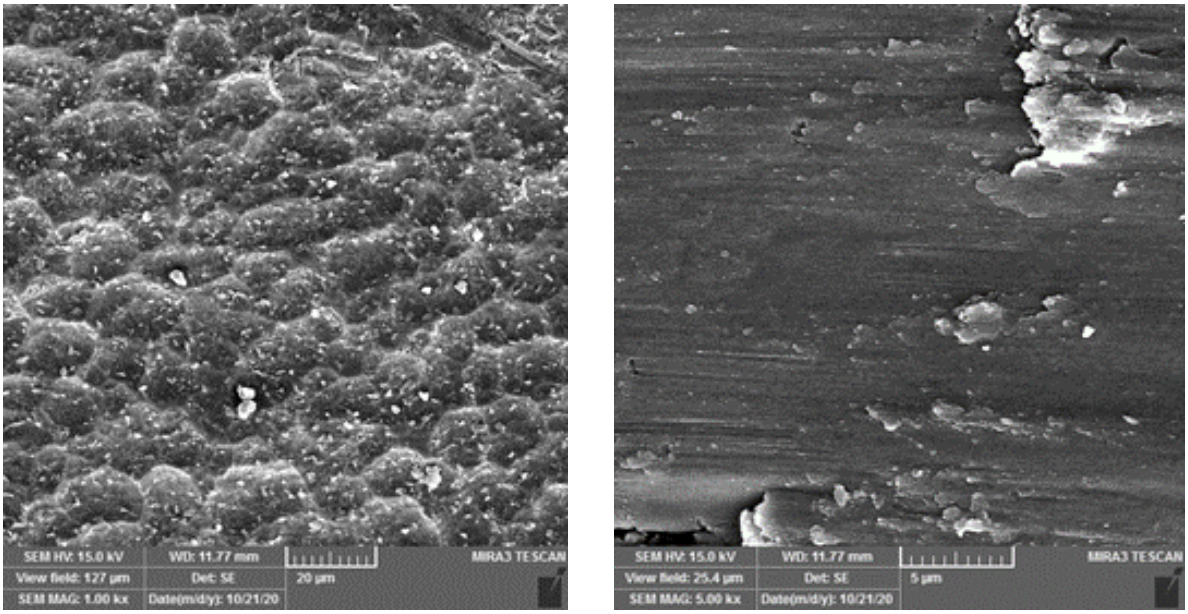

Fig. 11. shows an image of the reference sample surface after abrasion testing at a constant load of 300 g and a distance of 50 m, (a) before wear (b) after wear

[DOI: 10.22068/ijmse.2639]

This has resulted in an increase in the surface area of aluminum, a decrease in hardness, and an increase in the coefficient of friction. However, other factors can also be effective in the meantime, and these will be discussed in future sections.

Figure 13 illustrates how weight loss changes with spark energy. Weight loss is interestingly similar to changes in friction coefficients with spark energy. As can be seen in this figure, with increasing spark energy, the amount of weight loss increases, and the amount of this increase is approximately 28%. Also, the presence of more aluminum on the surface and its contact with the titanium pin can increase adhesive wear and result in greater weight loss.

In both the change of coefficient of friction and the change in weight loss of the specimens with spark energy, the greatest improvement or attenuation occurred around the energy of 5 joules. This is consistent with the results presented in the previous sections on hardness and roughness.

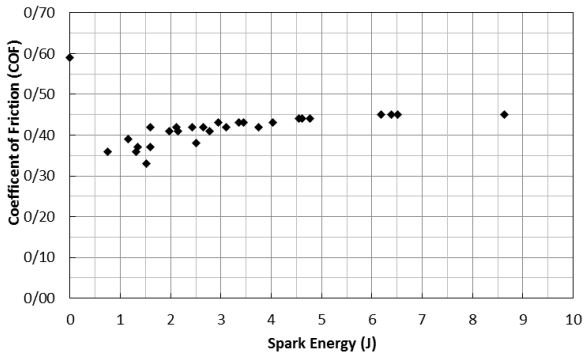

Fig. 12. Changes in the coefficient of friction with spark energy in wear under a load of 300 g force and a distance of 50 m.

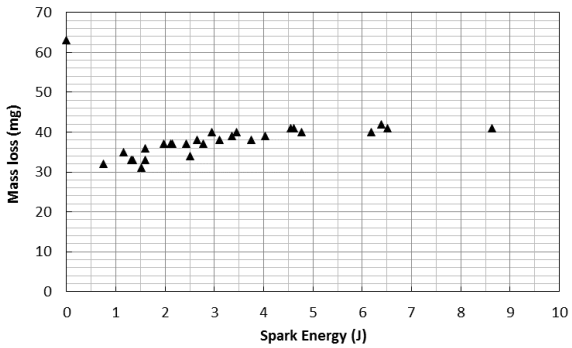

Fig. 13. Weight loss changes with spark energy in wear under a load of 300 g of force and a distance of 50 m.

Figure 14 illustrates how the volume reduction changes with spark energy. The variation in volume reduction is calculated using the theoretical density and weight reduction of samples. Therefore, its changes are quite similar to Figure 13.

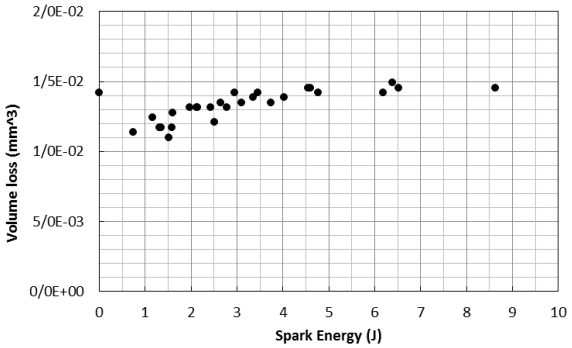

Fig. 14. Volume reduction changes with spark energy in wear under a load of 300 g force and a distance of 50 m.

Figure 15 shows the Lancaster coefficient variations with spark energy. Lancaster coefficient changes (as a coefficient without abrasion dimension) are calculated using Equation 2. In this figure, it can be seen that the changes in the the Lancaster coefficient are similar to the changes in the coefficient of friction, and the largest increase occurred around 5 joules of energy.

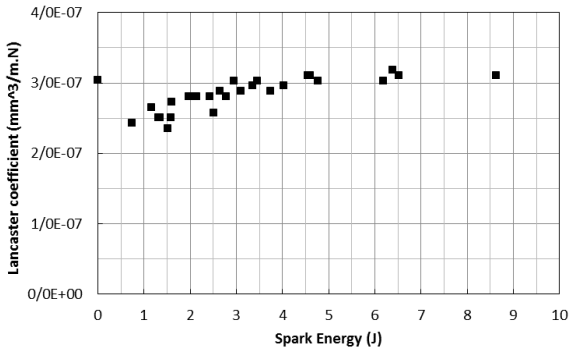

Fig. 15. Changes of Lancaster coefficient with spark energy in wear under the load of 300 g force and distance of 50 m.

Finally, Figure 16 shows the changes in wear rate with spark energy. This is also calculated using Equation 3-2. According to the figure, the Lancaster coefficient changes are similar to the changes in the coefficient of friction, and the largest increase occurred around 5 joules of energy. As can be seen in this figure, as spark energy

[DOI: 10.22068/ijmse.2639]

increases, the wear rate increases as well, and this increase is approximately 27%. As mentioned before, the reason for the increase in wear rate is probably the presence of more aluminum on the surface and the increase in sticky wear.

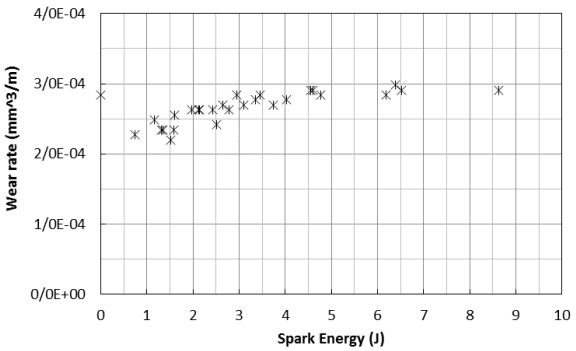

Fig. 16. Changes in wear rate with spark energy in wear under a load of 300 g force and a distance of 50 m.

To better understand the wear mechanism of the samples, their wear surface was also imaged with a scanning electron microscope. Still, to avoid the multiplicity of images presented, in this section, five sample categories were selected according to the important criteria for wear (such as coating thickness, roughness, and hardness), which are:

1. The first category: the sample with the lowest thickness (250860) and the sample with the highest thickness (251170),
2. The second category: the sample covered with the lowest roughness (150550) and the sample covered with the highest (351170),
3. The sample with the lowest surface hardness (351170) and the sample with the highest surface hardness (350550).

3.4.4.1 The first category: the effect of coating thickness on the wear rate

In this category, the sample with the lowest thickness (250860) and the sample with the highest thickness (251170) AH were selected to investigate the wear levels. Figure 17 shows the surface images of these samples after wear. As shown in the figure, the sample with the lowest thickness has practically lost its surface roughness after abrasion, and its surface is almost identical to the reference sample. It seems that due to the low thickness, the coating seems to be worn or peeled off the surface after a while. This is also well illustrated in Figure 17. The changes in coefficient of friction for this sample indicate that as the wear path has become longer, the coefficient of friction has also increased. This is probably due to the gradual removal of the coating from the surface. The presence of thin cracks on the surface also indicates the low thickness of the coating residue. In the sample with the highest thickness, however, the effects of wear have not yet reached the underlying layers of the coating, which indicates a positive effect of thickness.

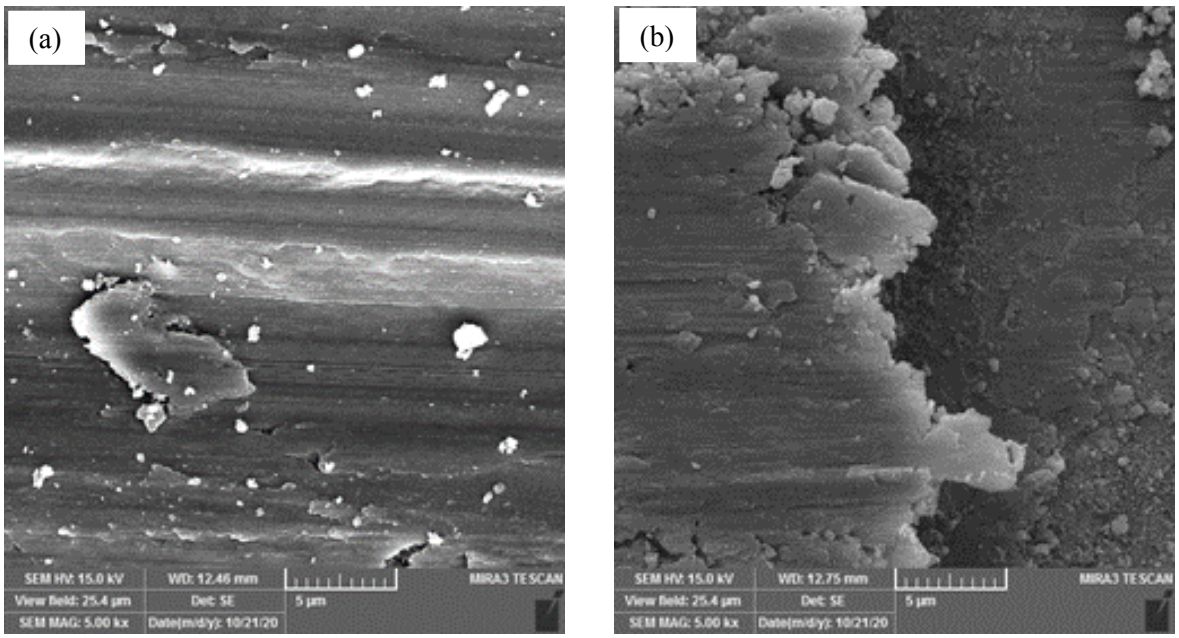

Fig. 17. Image of the sample surface (a) with the lowest thickness (250860) and (b) with the highest thickness (251170) after performing an abrasion test at a constant load of 300 g of force and a distance of 50 m.

[DOI: 10.22068/ijmse.2639]

The coefficient of friction did not change significantly along the wear path, which is most likely due to the presence of a coating along the path to the end of the test. However, the wear rate results of these two samples show that the wear rate of the sample with the lowest thickness is 4% less than the sample with the highest thickness. This can be the maximum thickness due to the high roughness of the sample. The wear mechanism in both samples is of the scratching mechanism type, and the wear path has no special effects of adhesive wear. The presence of fine particles separated from the surface is more obvious in the sample with the lowest thickness. This could be due to the fact that more coverage has been removed in this example. As expected, there are particles on the surface of the sample with the highest thickness, but the quantity of these particles is much less than the sample with the lowest thickness. Figure 18 illustrates a comparative study of the effect of coating thickness on wear rate. In addition, the results of this figure indicate that the wear rate increases with increasing coating thickness. Furthermore, the lowest wear rate occurs around 4 to 5 micrometers thick.

3.4.4.2 The second category: the effect of surface roughness on the wear rate

The effect of surface roughness on wear is discussed in this section. The sample with the lowest roughness (150550) and the sample with the highest roughness (351170) were selected as examples to demonstrate the results.

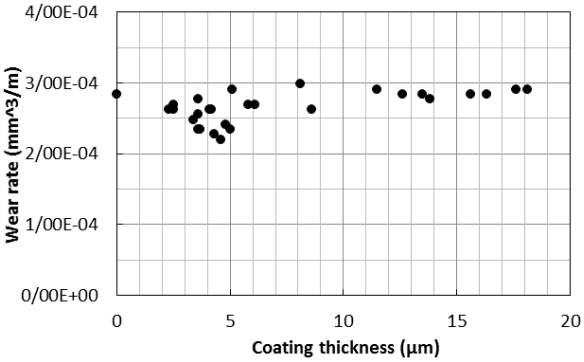

Fig. 18. Changes in wear rate with spark energy in wear under a load of 300 g force and a distance of 50 m.

Figure 19 illustrates the surface images of these samples after wear. Figure 19a illustrates how the sample with the lowest roughness has practically lost its surface morphology and is almost identical to the reference sample after wear. It seems that due to the low thickness, the coating seems to be worn or peeled off the surface after a while. This is probably due to the gradual removal of the coating from the surface. In reaching the pin to the substrate, we can intensify the adhesive wear mechanism and increase the coefficient of friction.

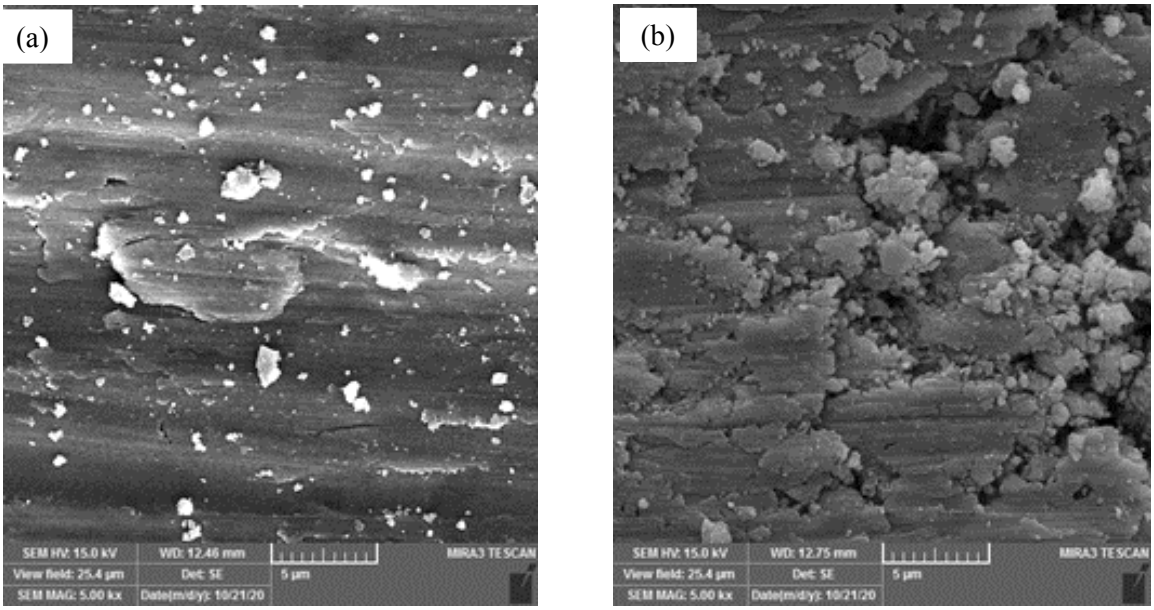

Fig. 19. Image of the sample surface (a) The sample with the lowest roughness (150550) and (b) The sample with the highest roughness (351170), after performing a wear test at a constant load of 300 g force and a distance of 50 meters.

[DOI: 10.22068/ijmse.2639]

The presence of thin cracks in the surface of sample 150550 also indicates this. There are also cracks visible on the surface of these samples, which are probably caused by the activation of adhesive wear mechanisms. However, in the sample with the highest roughness, it is evident that the effect of wear has not yet reached the underlying layers of the coating (Figure 19b). The coefficient of friction of this sample did not change significantly along the wear path, which is probably due to the presence of coatings along the wear path. However, in this sample, the coefficient of friction increases immediately after the onset of wear (Figure 20). This could be a result of the high roughness of the surface. However, the wear rates of two samples, 150550 and 351170, demonstrate that the wear rate of sample 351170 is 78% lower than that of sample 150550. This could be due to the higher stiffness of the 150550 sample. The predominant wear mechanism in both specimens is a scratch mechanism. The presence of fine particles isolated from the surface is evident in both samples.

Figure 20 illustrates the effect of roughness on wear rate. This figure also demonstrates that the wear rate increases as the surface roughness increases. As can also be seen, the lowest wear rate occurs at roughness levels of approximately 100 nm. This is probably due to the low hardness of the samples.

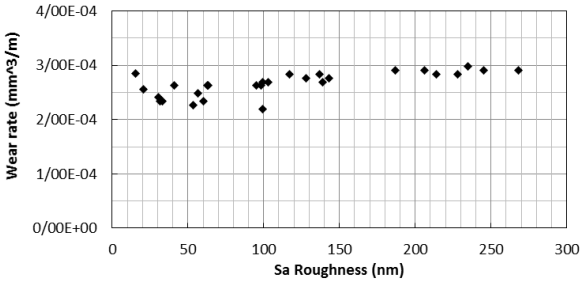

Fig. 20. Changes in wear rate with surface roughness in wear under the load of 300 g force and distance of 50 m.

3.4.4.3 Third category: the effect of surface hardness on the wear rate

In this section, the effect of surface hardness on wear is discussed. The sample with the lowest hardness (351170) and the sample with the highest hardness (350550) were selected as examples for the presentation of the results. The surface images of these samples are shown in Figure 21.

The sample surface, shown in Figure 24(a), has the lowest hardness after wear and shows both abrasive and adhesive abrasion. The abrasive abrasion can be caused by the presence of a coating on the surface of the sample since all samples with coating showed excellent resistance to abrasion.

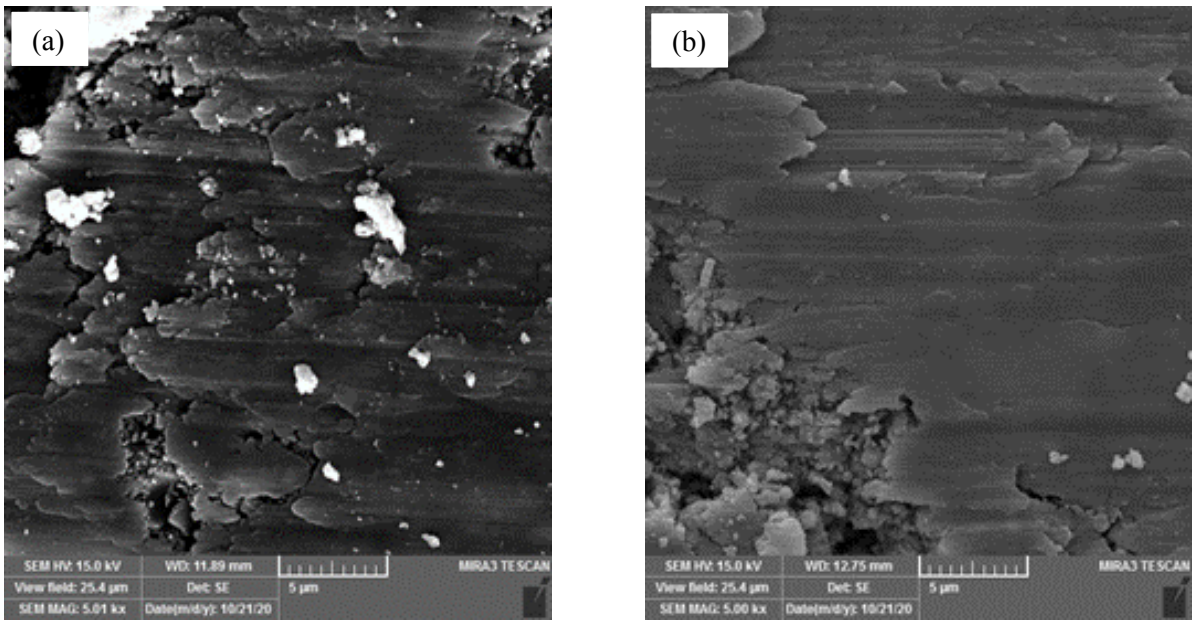

Fig. 21. Image of the sample surface (a) The sample with the lowest hardness (351170) and (b) The sample with the highest hardness (350550) after performing an abrasion test at a constant load of 300 g force and a distance of 50 meters.

[DOI: 10.22068/ijmse.2639]

The presence of adhesive wear may be related to the softness of the coating, its adhesion to the pin, and the removal of parts of the surface. As can be seen from Figure 21b, the sample with the highest hardness shows a relatively general change in surface morphology, but adhesive wear is not apparent. This can be attributed to two factors: higher surface hardness (up to 26%) and lower coating roughness (up to 32%). As the wear path increases (Figure 21), the coefficient of friction of sample 351170 increases and then decreases. Due to the low stiffness of the sample in the early stages of wear, the mechanism was mainly adhesive, but with increasing distance and stiffness due to possible plastic deformation, as well as the possibility of surface oxidation and increased stiffness locally. The coefficient of friction is reduced. The presence of some cracks in the surface can be due to this oxidation. However, the coefficient of friction of the sample has the lowest hardness of approximately 36% more than the coefficient of friction of the sample has the highest hardness. There are also cracks on the surface of this sample, which are probably caused by the activation of surface oxidation. The wear rates of samples 350550 and 351170 show that the sample 350550 wears at a rate that is 75% lower than the sample 351170. This could be due to the higher stiffness of the 350550 sample. The presence of fine particles isolated from the surface is evident in both samples.

Figure 22 depicts the effect of hardness on wear rate. The results of this figure indicate that the wear rate decreases with increasing surface hardness.

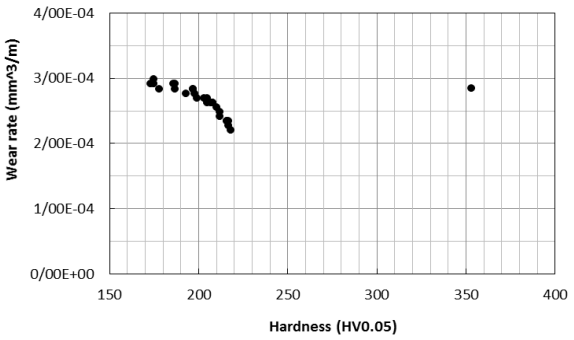

Fig. 22. Changes in wear rate with difficulty in wear under a load of 300 g force and a distance of 50 m.

The lowest wear rate can also be seen around the hardness of 220 Vickers. These changes could also be predicted using 1 and 2 relationships. According to these relationships, the wear rate is inversely related to the hardness.

3.4.5. Investigation of Lancaster coefficient changes with surface parameters

The advantage of using the Lancaster coefficient instead of the Archard wear coefficient (dimensionless wear coefficient) is that there is no need for hardness values to calculate the wear rate. Few studies have been conducted on the factors affecting this coefficient; therefore, in this study, for the first time, the effect of surface parameters, such as roughness, hardness, and coating thickness, on the Lancaster coefficient was studied, and an equation was presented to predict it. Figure 23 shows the changes in Lancaster coefficient with thickness, roughness, and hardness of the coating in wear under a load of 300 g of force and a distance of 50 m. As can be seen from this figure, the Lancaster coefficient increases by approximately 35% when the coating thickness is increased from 3 to 18 μm. Regarding the changes of the Lancaster coefficient with difficulty, it can be seen that this coefficient decreases with increasing accuracy exactly following the wear rate. In order to determine the exact effect of these three surface variables on the Lancaster coefficient, the Fourier series expansion was used (Equation 3).

$$d\mathrm{k}' = \frac{\partial \mathrm{k}'}{\partial \mathrm{x}}\mathrm{dx} + \frac{\partial \mathrm{k}'}{\partial \mathrm{S_a}}\mathrm{dS_a} + \frac{\partial \mathrm{k}'}{\partial \mathrm{H}}\mathrm{dH} + \frac{\partial^2 \mathrm{k}'}{\partial \mathrm{x}^2}(\mathrm{dx})^2 + \frac{\partial^2 \mathrm{k}'}{\partial \mathrm{S_a}^2}(\mathrm{dS_a})^2 + \frac{\partial^2 \mathrm{k}'}{\partial \mathrm{H}^2}(\mathrm{dH})^2 + \frac{\partial^2 \mathrm{k}'}{\partial \mathrm{x}\,\partial \mathrm{S_a}}\mathrm{dx dS_a} + \frac{\partial^2 \mathrm{k}'}{\partial \mathrm{x}\,\partial \mathrm{H}}\mathrm{dx dH} + \frac{\partial^2 \mathrm{k}'}{\partial \mathrm{H}\,\partial \mathrm{S_a}}\mathrm{dH dS_a} + \cdots \quad (3)$$

In this regard, k′ (mm^3/m.N) is Lancaster coefficient, x (μm) is the thickness of the coating, S_a (nm) is the surface roughness and H (HV0.05) is the surface hardness. Given the small values of k′ and assuming that the changes in hardness, roughness and thickness are small together, second- and higher-degree derivatives can be discarded. Therefore, the following relationship will remain:

$$d\mathrm{k}' = \frac{\partial \mathrm{k}'}{\partial \mathrm{x}}\mathrm{dx} + \frac{\partial \mathrm{k}'}{\partial \mathrm{S_a}}\mathrm{dS_a} + \frac{\partial \mathrm{k}'}{\partial \mathrm{H}}\mathrm{dH} \quad (4)$$

By integrating Equation 3-4, Equation 3-5 is obtained:

$$\mathrm{k}' = \int \frac{\partial \mathrm{k}'}{\partial \mathrm{x}}\mathrm{dx} + \int \frac{\partial \mathrm{k}'}{\partial \mathrm{S_a}}\mathrm{dS_a} + \int \frac{\partial \mathrm{k}'}{\partial \mathrm{H}}\mathrm{dH} \quad (5)$$

As a result of utilizing Equation 3-5 and the results presented in Figure 23, MINITAB software can be used to determine the best equation governing

[DOI: 10.22068/ijmse.2639]

the behavior of the Lancaster coefficient.

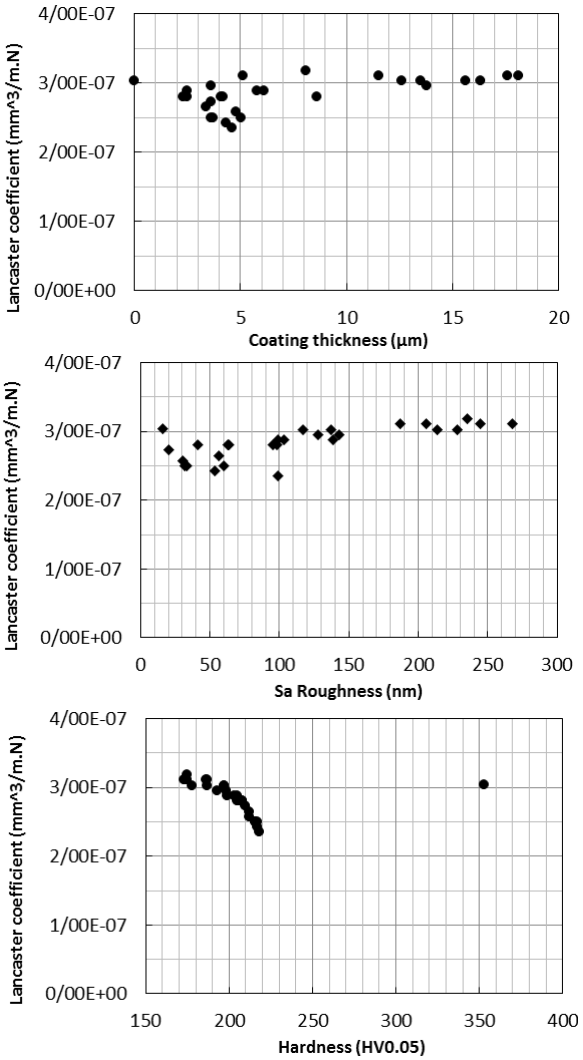

Fig. 23. Illustrates the changes in Lancaster coefficient with thickness, roughness, and hardness of coatings under 300 g load and a distance of 50 m.

Accordingly, this software predicts changes in the Lancaster coefficient based on three variables: roughness, thickness, and hardness 3-6.

$$k' = -1.91 \times 10^{-11}x^2 + 9.74 \times 10^{-10}x - 4.42 \times 10^{-16}S_a^2 + 4.42 \times 10^{-11}S_a - 1.11 \times 10^{-11}H^2 + 4.42 \times 10^{-9}H - 1.66 \times 10^{-7} \quad (6)$$

Software calculations show that unlike Equation 2, changes in the Lancaster coefficient are directly related to H^2 in addition to H. In order to validate the results, all samples were calculated again using Lancaster ratio 6 and the error rate was obtained. These values are shown in Table 5. As can be seen, the proposed model provides a relatively accurate forecast of 5.5% for all samples with relatively accurate prediction coverage, which is relatively acceptable. The reason for the high error in reference samples is the lack of coating on them and zeroing of the coefficients of variable thickness of the coating (x). Another cause of the error could be the use of µm units for thickness instead of mm, nm for surface roughness instead of mm, and HV0.05 for surface hardness instead of N/mm^2. The reason for using these units was that they were common in measuring the relevant variable. Changing the units causes the coefficients of the variables to increase and the error of the numbers to decrease.

4. CONCLUSIONS

The general results of this research can be summarized as follows:

- SEM images confirmed the formation of aluminum/molybdenum disulfide nanocomposite coatings on the substrate surface.
- XRD analysis showed that in addition to the metallic titanium phase, peaks related to the Al, MoS_2, and Al_2O_3 phases could also be observed on the surface.
- The hardness of the reference sample is 353 Vickers, but the surface hardness of almost all coated samples is about 200 Vickers. Because the Al/MoS_2 coating is generally less hard than the titanium substrate.
- The roughness of a surface generally increases with an increase in spark energy. The roughness of the coated sample ranges from 15.7 nm for the reference sample to 268.1 nm using the highest spark energy (351170).
- The wear rate increases with an increase in spark energy. As spark energy increases, the coefficient of friction increases, and this increase is approximately 0.09 and 25%. Increasing the spark energy and spraying the molten droplets increases the likelihood of MoS_2 particles separating from the surface. This has resulted in an increase in the surface area of aluminum metal, a decrease in its hardness, and an increase in the coefficient of friction.
- The Lancaster coefficient changes similar to the coefficient of friction, with the greatest increase occurring at approximately five joules of energy.
- The wear rate increases with an increase in spark energy, and the amount of this increase

[DOI: 10.22068/ijmse.2639]

- is approximately 27%. The increase in wear rate may be caused by the presence of more aluminum on the surface and increased adhesive wear.
- The amount of weight loss increases as the spark energy level increases, resulting in an increase of approximately 28%. More aluminum on the surface and its contact with the titanium pin can increase adhesive wear and result in more weight loss.
- The results of the wear rate tests indicate that the wear rate for the sample with the lowest thickness is 4% less than that of the sample with the highest thickness.
- As a result of wear, the sample with the lowest roughness has lost its surface morphology, and its surface is nearly identical to that of the reference sample. Due to the lesser thickness, the coating is worn or peeled off the surface after a while. By reaching the pin to the substrate, the adhesive wear mechanism is intensified, and the coefficient of friction increases. The comparison of the wear rates of samples 150550 and 351170 shows that the wear rate for sample 351170 is 78% lower than that of sample 150550.
- The surface of the sample with the lowest post-abrasion hardness has both abrasive and adhesive abrasion effects. In comparison with the two samples, 350550 and 351170, the wear rate of the sample 350550 is 75% lower than the wear rate of sample 351170. This could be due to the higher stiffness of the 350550 sample.
- The equations of Lancaster coefficient changes were extracted and validated by considering roughness, coating thickness, and surface hardness.

Table 5. shows the values and error rates of the Lancaster coefficients calculated and predicted for different samples.

sample code	Calculated	Predicted	Error (%)
Ref.	3.04e-07	2.84e-04	-94.6
150550	2.43e-07	2.27e-04	14.8
250550	2.50e-07	2.34e-04	11.2
350550	2.35e-07	2.20e-04	19.3
150850	2.65e-07	2.48e-04	5.3
250850	2.80e-07	2.63e-04	0.8
350850	2.80e-07	2.63e-04	0.3
151150	2.73e-07	2.56e-04	2.1
251150	2.80e-07	2.63e-04	-0.4
351150	2.88e-07	2.70e-04	-0.5
150560	2.50e-07	2.34e-04	10.9
250560	2.80e-07	2.63e-04	1.4
350560	2.88e-07	2.70e-04	-1.0
150860	2.80e-07	2.63e-04	0.3
250860	3.03e-07	2.84e-04	-4.0
350860	3.03e-07	2.84e-04	-3.1
151160	3.03e-07	2.84e-04	-4.4
251160	3.11e-07	2.91e-04	-7.7
351160	3.11e-07	2.91e-04	-6.4
150570	2.50e-07	2.34e-04	11.3
250570	2.88e-07	2.70e-04	-2.1
350570	2.96e-07	2.77e-04	-3.7
150870	2.58e-07	2.41e-04	8.4
250870	3.11e-07	2.91e-04	-6.5
350870	3.18e-07	2.98e-04	-10.2
151170	2.96e-07	2.77e-04	-1.6
251170	3.03e-07	2.84e-04	-4.1
351170	3.11e-07	2.91e-04	-6.5
Mean squared error (R^2) excluding reference sample			5.5

[DOI: 10.22068/ijmse.2639]

REFERENCES

[1] Fellah M., Hezil N., Touhami M.Z., AbdulSamad M., Obrosov A., Bokov D.O., "Structural, tribological and antibacterial properties of (α + β) based ti-alloys for biomedical applications", J. Mater. Res. Technol., 2020, 9:140, 61–74.

[2] Longhitano G.A., Larosa M.A., Jardini A.L., Zavaglia C.A. de C., Ierardi M.C.F, "Correlation between microstructures and mechanical properties under tensile and compression tests of heat-treated Ti-6Al–4 V ELI alloy produced by additive manufacturing for biomedical applications", J. Mater. Process. Technol., 2018, 252:20, 2–10.

[3] Behera R.R., Das A., Hasan A., Pamu D., Pandey L.M., Sankar M.R., "Deposition of biphasic calcium phosphate film on laser surface textured Ti–6Al–4V and its effect on different biological properties for orthopedic applications", J. Alloys Compd., 2020, 842, 155683.

[4] De Oliveira V.M.C.A., Da Silva M.C.L., Pinto C.G., Suzuki P.A., Machado J.P.B., Chad V.M., "Short-term creep properties of Ti-6Al-4V alloy subjected to surface plasma carburizing process", J. Mater. Res. Technol., 2015, 4:3, 59–66.

[5] Guo R., Xu L., Wu J., Yang R., Zong B.Y., "Microstructural evolution and mechanical properties of powder metallurgy Ti-6Al-4V alloy based on heat response", J. Mater. Sci. Eng. A, 2015, 639:3, 27–34.

[6] Chen C., Feng X., Shen Y., "Synthesis of Al–B4C composite coating on Ti–6Al–4V alloy substrate by mechanical alloying method", J. Surf. Coatings Technol., 2017, 321, 8–18.

[7] Mohseni E., Zalnezhad E., Bushroa A.R., "Comparative investigation on the adhesion of hydroxyapatite coating on Ti-6Al-4V implant: A review paper", Int. J. Adhes. Adhes. 2014, 48:2, 38–57.

[8] Velay V., Matsumoto H., Vidal V., Chiba A., "Behavior modeling and microstructural evolutions of Ti-6Al-4V alloy under hot forming conditions", Int. J. Mech. Sci., 2016, 108–109, 1–13.

[9] Oskooie M.S., Motlagh M.S., Aghajani H., "Surface properties and mechanism of corrosion resistance enhancement in a high temperature nitrogen ion implanted medical grade Ti", J. Surf. Coatings Technol., 2016, 291:3, 56–64.

[10] Aghajani H., Motlagh M.S., "Effect of temperature on surface characteristics of nitrogen ion implanted biocompatible titanium", J. Mater. Sci. Mate.r Med. 2017, 28, 1–10.

[11] Tijo D., Masanta M., Das A.K., "In-situ TiC-TiB2 coating on Ti-6Al-4V alloy by tungsten inert gas (TIG) cladding method: Part-I. Microstructure evolution", J. Surf. Coatings Technol., 2018, 344:5, 41–52.

[12] Sandeep Reddy A.V., Ajay Kumar S., Jagadesh T., "The Influence of graphite, MOS_2 and Blasocut lubricant on hole and chip geometry during peck drilling of aerospace alloy", J. Mater. Today Proc., 2020, 24:6, 90–97.

[13] Suarez M.P., Marques A., Boing D., Amorim F.L., Machado Á.R., "MoS_2 solid lubricant application in turning of AISI D6 hardened steel with PCBN tools", J. Manuf. Process, 2019, 47:3, 37–46.

[14] Charoo M.S., Wani M.F., Hanief M., Rather M.A., "Tribological Properties of MoS_2 Particles as Lubricant Additive on EN31 Alloy Steel and AISI 52100 Steel Ball", J. Mater. Today Proc., 2017, 4:99, 67–71.

[15] Wang Y., Du Y., Deng J., Wang Z., "Friction reduction of water based lubricant with highly dispersed functional MoS_2 nanosheets", J. Colloids Surfaces A. Physicochem. Eng. Asp., 2019, 562:32, 1–8.

[16] Hong J., Hu Z., Probert M., Li K., Lu D., Yang X., "Exploring atomic defects in molybdenum disulphide monolayers", J. Nat. Commun., 2015, 6, 1–8.

[17] Castellanos-Gomez A., Poot M., Steele G.A., Van Der Zant H.S.J., Agraït N., Rubio-Bollinger G., "Elastic properties of freely suspended MoS_2 nanosheets", J. Adv. Mater., 2012, 24:77, 2–5.

[18] Vazirisereshk M.R., Martini A., Strubbe D.A., Baykara M.Z., "Solid lubrication with MoS2: A review", J. Lubricants, 2019, 7.

[19] Kanthavel K., Sumesh K.R., Saravanakumar P., "Study of tribological

[DOI: 10.22068/ijmse.2639]

properties on Al/Al_2O_3/MoS_2 hybrid composite processed by powder metallurgy", Alexandria Eng. J., 2016, 55:1, 3–7.
[20] Su Y., Zhang Y., Song J., Hu L., "Novel Approach to the Fabrication of an Alumina-MoS_2 Self-Lubricating Composite via the in Situ Synthesis of Nanosized MoS_2", A.C.S. Appl. Mater. Interfaces, 2017, 9:30, 263–266.
[21] Li L., Lu Z., Pu J., Wang H., Li Q., Chen S., "The superlattice structure and self-adaptive performance of C–Ti/MoS_2 composite coatings", J. Ceram. Int., 2020, 46:57, 33–44.
[22] Li L., Lu Z., Pu J., Hou B., "Investigating the tribological and corrosive properties of MoS_2/Zr coatings with the continuous evolution of structure for high-humidity application", J. Appl. Surf. Sci., 2021, 541.
[23] Peng Z., Cheng T., Nie X., "MoS_2/Al_2O_3 composite coatings on A356 alloy for friction reduction", J. Adv. Mater. Res., 2012, 496:4, 88–92.
[24] Razavi Arab S.J., Aghajani H., "Wear Behavior of Pure Titanium Coated With WC-Co by the Use of Electrospark Deposition Method", J. Tribol., 2019, 141, 3–9.
[25] Azhideh M., Aghajani H., Pourbagheri H., "Surface characterization and corrosion resistance of 36Cr-Ni-Mo_4 steel coated by WC-Co cermet electrode using micro-electro welding", J. Metals, 2017, 7(8), 308-325.
[26] Reynolds Jr. J.L., Holdren R.L., Brown L.E., "Electro-spark deposition: electro-spark deposition is a viable process suitable for applying overlays and restoring part dimensions with little effect on the substrate microstructure", J. Adv. Mater. Process., 2003, 161, 35.
[27] Frangini S., Masci A., "A study on the effect of a dynamic contact force control for improving electrospark coating properties", J. Surf. Coatings Technol., 2010, 204:26, 13–23.
[28] Hong X., Tan Y.F., Wang X.L., Tan H., Xu T., "Effects of nitrogen flux on microstructure and tribological properties of in-situ TiN coatings deposited on TC11 titanium alloy by electrospark deposition", J. Trans. Nonferrous Met. Soc. China, 2015, 25:33, 29–38.
[29] Chang-Bin T., Dao-Xin L., Zhan W., Yang G., "Electro-spark alloying using graphite electrode on titanium alloy surface for biomedical applications", J. Appl. Surf. Sci., 2011, 257:63, 64–71.
[30] HUTCHINGS I.M., "Tribology: friction and wear of engineering materials", Edward Arnold (ed.), St., 1992, 22-85.
[31] Tabrizi A.T., Aghajani H., Saghafian H., Laleh F.F., "Correction of Archard equation for wear behavior of modified pure titanium", J. Tribol. Int., 2021, 155, 106772.
[32] Fellah M., Labaïz M., Assala O., Dekhil L., Taleb A., Rezag H., "Tribological behavior of Ti-6Al-4V and Ti-6Al-7Nb Alloys for Total Hip Prosthesis", J. Adv. Tribol., 2014, 451387.
[33] Łkepicka M., Grkadzka-Dahlke M., "Surface modification of Ti_6Al_4V Titanium Alloy for Biomedical Applications and Its Effect an Tribological Performance-A Review", J. Rev. Adv. Mater. Sci., 2016, 46, 86-103.

[DOI: 10.22068/ijmse.2639]